Restoring the Suzaku Source Position Accuracy and Point-Spread Function

Yasunobu Uchiyama,[1] Yoshitomo Maeda,[1] Masatoshi Ebara,[1]
Ryuichi Fujimoto,[2] Yoshitaka Ishisaki,[3] Manabu Ishida,[1]
Ryo Iizuka,[1,4] Masayoshi Ushio,[1] Hirohiko Inoue,[1]
Shunsaku Okada,[1] Hideyuki Mori,[5] and Masanobu Ozaki[1]

[1]*Department of High Energy Astrophysics, Institute of Space and Astronautical Science (ISAS),*
Japan Aerospace Exploration Agency (JAXA), 3-1-1 Yoshinodai, Sagamihara, 229-8510
[2]*Graduate School of Natural Science and Technology, Kanazawa University,*
Kakuma-machi, Kanazawa, 920-1192
[3]*Department of Physics, Tokyo Metropolitan University,*
1-1 Minami-Osawa, Hachioji, Tokyo 192-0397
[4]*Nishi-Harima Astronomical Observatory,*
407-2 Nishikawauchi, Sayo-cho, Sayo-gun, Hyogo, 679-5313
[5]*Department of Physics, Kyoto University, Sakyo-ku, Kyoto 606-8502*

Abstract

We present an empirical correction of sky coordinates of X-ray photons obtained with the X-ray Imaging Spectrometer (XIS) aboard the Suzaku satellite to improve the source position accuracy and restore the point-spread function (PSF). The XIS images are known to have an uncertainty in position of up to $1'$, and to show considerable degradations of the PSF. These problems are caused by a drifting of the satellite attitude due to thermal distortion of the side panel #7, where the attitude control system is mounted. We found that the position error averaged over a pointing observation can be largely reduced by using the relation between the deviation of the source position in the DETX direction and the ecliptic latitude of the pointing target. We parameterized the wobbling of the source position synchronized with the 96-minute satellite orbital period with temperatures of onboard radiators and elapsed time since the night-day transition of the spacecraft. We developed software, aeattcor, to correct the image drift using these parameters, and applied it to 27 point-source images taken in the Suzaku initial science-operation phase. We show that the radius of the 90% error circle of the source position was reduced to $19''$ and the PSF was sharpened. These improvements have enhanced the scientific capability of the Suzaku XIS.

Key words: instrumentation: miscellaneous — space vehicles: instruments — X-rays: general

1. Introduction

The X-ray Observatory Suzaku (Mitsuda et al. 2007), developed jointly by Japan and the US, has two active scientific payload, XIS (X-ray Imaging Spectrometer: Koyama et al. 2007) and HXD (Hard X-ray Detector: Takahashi et al. 2007). XIS consists of four X-ray imaging CCD cameras covering a field-of-view of $17'\!\!.8 \times 17'\!\!.8$; three are front-illuminated (0.4–12 keV), and one is a back-illuminated CCD (0.2–12 keV). The XISs are located on the focal plane of the X-ray Telescopes, XRTs (Serlemitsos et al. 2007). Each X-ray photon recorded by the XIS can be localized with the CCD native pixels, each of which has dimensions of $1.04'' \times 1.04''$. While the PSF of the XRTs has a broad distribution with a half-power diameter (HPD) of $\sim 2'$, it has a sharp core with a width of $\sim 10''$. Thus, the sky positions of point-like sources with good photon statistics ($\gtrsim 10^4$ photons) are in principle determined with a precision of better than $\sim 10''$, if we know the instantaneous pointing direction of the XRT perfectly. The positional information is crucial to search for coun-

terparts in other wavelengths [e.g., a new supersoft source discovered by Suzaku; see Takei et al. (2007)] and also to construct source catalogs [e.g., Ueda et al. (2001) and Ueda et al. (2005) in the case of ASCA].

The celestial coordinates of each photon detected with the Suzaku XRT-XIS are calculated from the position coordinates of the CCD pixels defined on the XRT focal plane and the instantaneous pointing direction of the XRT. The arcsecond localizations of optical guide stars by a pair of star trackers (STTs) primarily determine the absolute pointing direction of the XRT. While guide stars are not available, a set of gyroscopes takes a role to determine the pointing direction. However, over the course of in-orbit calibrations of the Suzaku XRT, it was revealed that the calculated positions of X-ray sources have an error of $1'$ (Serlemitsos et al. 2007), which is significantly larger than that expected in the pre-flight specifications, $\sim 10''$. The deviation of the calculated source position from the true position is time-dependent and synchronized with the orbital motion of the spacecraft. Its behavior differs from one observation to another. The error of the

source position can be as large as $1'$, and therefore the astrometric accuracy of the XIS images has been taken to be $\sim 1'$ so far.

The cause of this problem has been identified with a thermal distortion of the satellite chassis, particularly the cross frames on the side panel #7 (see figure 1), as briefly stated in Serlemitsos et al. (2007). This panel is situated on the anti-Sun side of the spacecraft, where the dewar of the X-ray Spectrometer (XRS: Kelley et al. 2007) is placed. To expose the XRS dewar to space, the lower half of the panel #7 is skeletonized by cross frames made of aluminum [see figure 1 and also Mitsuda et al. (2007)]. The cross frames suffer from thermal distortion due mainly to Earth albedo illumination. Specifically, side panel #7 is forced to be tilted in the DETY direction as the cross frames expand, since the upper end of the panel is fixed at the side panels #6 and #8. Since the STT and gyroscopes are co-located on side panel #7, it causes a time-dependent misalignment between the XRT-XIS system and the attitude system, and consequently drifts the XRT pointing in the DETY direction. Also, an imbalance of thermal expansion between the cross frames induces rotation around the Y-axis (perpendicular to the side panel #7), resulting in drifts in the DETX direction.

We have investigated the characteristics of drift of the X-ray images to restore the pointing accuracy as close to the pre-flight specification as possible. Suzaku does not have onboard sensors for the temperatures of the cross frames, which are considered to be the most relevant parameters to the thermal distortion. We therefore have searched for relevant key parameters within the limited housekeeping data available on ground.

In the present work, we parameterize the drifts of the XRT pointing direction against the attitude control system with the spacecraft temperatures, the satellite orbital phase, and the average pointing direction relative to the ecliptic plane, and found a method to correct the position accuracy and the PSF in the observed XIS image using these parameters. We applied the method to point-source images taken in the initial scientific operation phase and derived the position accuracy currently achievable. The outline of this paper is as follows. We describe the data sets and basic reduction in section 2. The parameterization of drifts of the XRT pointing is presented in section 3, which is followed by a brief description of new software, aeattcor, developed for the position-error correction in section 4. We present the improvement on the PSF and the position accuracy in section 5. A summary is in section 6.

2. Observations

We analyzed XIS data acquired during the Suzaku initial science-operation phase for the present work. We selected data of point sources whose celestial coordinates were cataloged with a precision of better than a few arcseconds, their X-ray fluxes were higher than 0.5 counts s^{-1} chip^{-1}, but less than 100 counts s^{-1} chip^{-1} because a too-high count-rate caused a significant pileup
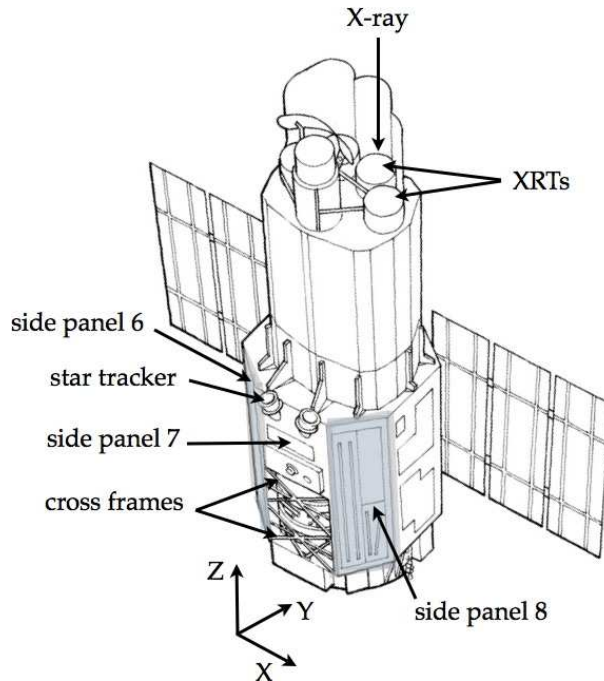
Fig. 1. Schematic view of the Suzaku satellite. Some key components in this work are indicated by arrows. Side panels #6 and #8 are indicated by grey shaded areas. The spacecraft (S/C) XYZ directions are shown. The DETX direction coincides with the S/C +X direction, while DETY is defined by the S/C −Y direction.

at the peak of the PSF and degraded the precision of the position determination.

Table 1 lists the selected X-ray sources, consisting mainly of active galactic nuclei and X-ray binaries, used in this work. (For multi-epoch monitoring observations, we used only the data of the two latest epochs in order not to enhance statistical weights on these sources.) We retrieved the Suzaku XIS data with version 1.2 pipeline processing (V1.2), and utilized cleaned event data. We analyzed the XIS images using sky coordinates, X/Y columns (+X is directed to west and +Y is north) in the event files, which were calculated from the detector coordinates (DETX/Y) of the CCD pixels and the satellite attitude monitored by the STTs and gyroscopes (Ishisaki et al. 2007). It is worth emphasizing that prior to the pipeline processing V1.0, the attitude determination with STTs and gyroscopes on ground had not been applied. We present results obtained from XIS-0, one of the three front-side illuminated CCDs, because the XIS-0 has the best PSF suited for our purpose. The drifts of all four XIS images due to the drifts of the satellite attitude were found to be almost identical. The results from XIS-0 are equally applicable to the other XIS data.

3. Analysis

3.1. Position Drift of Suzaku XIS Image

In order to track a drift of a source position in the sky coordinates (X/Y), we determined the quasi-

instantaneous peak of the sky image for every 200 second time bin by a two-dimensional Lorentzian fitting. The deviation of the peak position from the *expected* position $(\Delta X, \Delta Y)$ was computed at each time bin. The expected pixel position is (768.5, 768.5) if the source was aimed to be placed at the XIS nominal position. They were then converted into the detector coordinate system, $(\Delta X_{\mathrm{det}}, \Delta Y_{\mathrm{det}})$, using the following transformation:

$$\Delta X_{\mathrm{det}} = \Delta X \cos\theta + \Delta Y \sin\theta \tag{1}$$

$$\Delta Y_{\mathrm{det}} = -\Delta X \sin\theta + \Delta Y \cos\theta, \tag{2}$$

where θ is the average roll angle, PA_NOM, stored in the event file headers. A similar method was adopted in Gotthelf et al. (2000) for correcting the ASCA position accuracy.

To illustrate the characteristics of the drift of the XIS images, the time history of a source position obtained from data of Her X-1 (seq# 100035010) is shown in figure 2. It can be seen that the source position oscillates with amplitudes of $10''$–$30''$ in both ΔX_{det} and ΔY_{det} synchronized with the satellite orbital motion of a 96-min period. Furthermore, the center of oscillation has an offset toward the $-\Delta X_{\mathrm{det}}$ direction by $\sim 40''$, which causes a large astrometric error in the Suzaku XRT-XIS system.

We found that the position drift of the Suzaku XIS image can be well described by a wobbling motion synchronized with the satellite orbital motion and an offset which changes slowly in a much longer timescale than the orbital period during a fixed pointing observation. The offset appears to differ from one pointing to another. We derived the offset in both the X_{det} and Y_{det} directions for each pointing by fitting the time-integrated XIS image with a two-dimensional Gaussian function. We denote the derived offsets as $\langle\Delta X_{\mathrm{det}}\rangle$ and $\langle\Delta Y_{\mathrm{det}}\rangle$, though these quantities are not necessarily the average of the above deviations ΔX_{det} and ΔY_{det}. The offsets would be a good measure of the center of oscillation.

In the left panel of figure 3 we show a scatter plot of the offset, $\langle\Delta X_{\mathrm{det}}\rangle$ versus $\langle\Delta Y_{\mathrm{det}}\rangle$, derived for all of our samples. This plot represents the position accuracy of the Suzaku XIS image processed by the pipeline V1.2. We found that the dispersion of the offsets is larger in the DETX (X_{det}) direction, $\sim 70''$. The dispersion of the offset in the DETY direction is relatively small and the distribution tends to be positive.

3.2. Parametrization of Drift

We searched for related parameters to the offset and the wobbling motion of the X-ray image to recover the image that should be obtained in a condition free from the drift of the satellite attitude. We here assume that the long-timescale offset is constant during a fixed pointing observation.

3.2.1. Long-timescale offset

First, we found that the offset in DETX, $\langle\Delta X_{\mathrm{det}}\rangle$, has a clear correlation with the ecliptic latitude of the source, β_{ecl}. In figure 4 we present the distribution of $\langle\Delta X_{\mathrm{det}}\rangle$ of each observation against β_{ecl}. A linear relation between the DETX offset $\langle\Delta X_{\mathrm{det}}\rangle$ and the ecliptic latitude β_{ecl} is
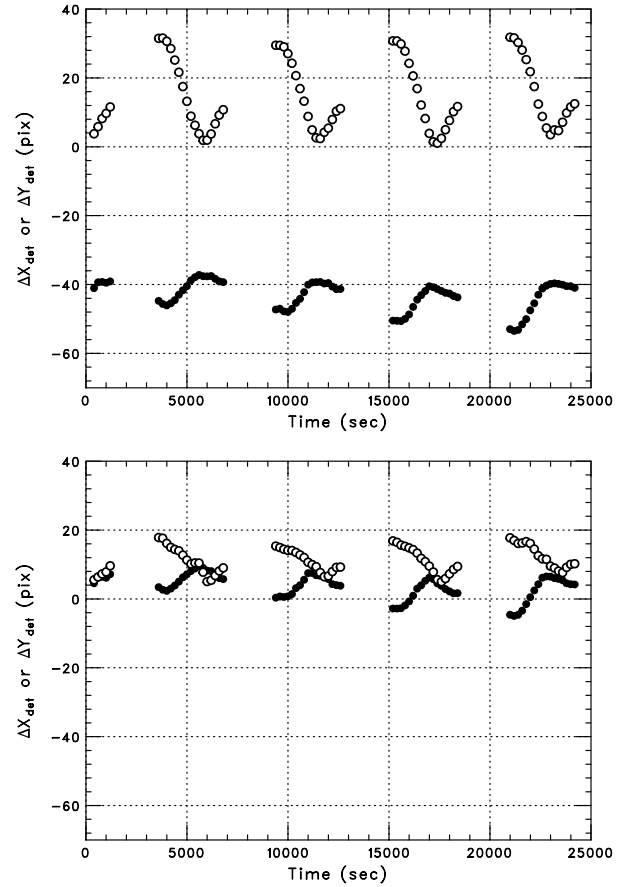

Fig. 2. (Top) Time sequence of ΔX_{det} (filled circles) and ΔY_{det} (open circles) in the case of Her X-1. One pixel corresponds to $\simeq 1.04''$. The origin of the source position is its nominal position, at which a source is expected to fall. (Bottom) Same as the top panel, but after the attitude-error correction (see subsection 3.2).

clearly seen. The ecliptic latitude β_{ecl} represents the angle of the XRT pointing direction from the ecliptic plane, and characterizes the way of illumination by the bright Earth. The strong correlation suggests that the geometry between the Sun, Earth, and the satellite, plays an essential roll in determining the long-timescale offset of the XRT pointing in the DETX direction. The configuration of side panel #7 relative to the ecliptic plane is considered to somehow control the thermal distortion of the cross frames.

The following linear relation is found to reasonably fit these data:

$$\langle\Delta X_{\mathrm{det}}\rangle(\beta_{\mathrm{ecl}}) = -38.5 \left(\frac{\beta_{\mathrm{ecl}}}{60 \ \mathrm{deg}}\right) - 9.25 \ \ \mathrm{pixels}. \tag{3}$$

This relation gives a DETX offset for a given observation using the ecliptic latitude of the target. It can be seen that $\langle\Delta X_{\mathrm{det}}\rangle \simeq 0$ for $\beta_{\mathrm{ecl}} \simeq -14°$. This is simply because the nominal position has been calibrated by MCG−6−30-15 (seq# 100004010), which has an ecliptic latitude of $\beta_{\mathrm{ecl}} \simeq -22.\!°5$.
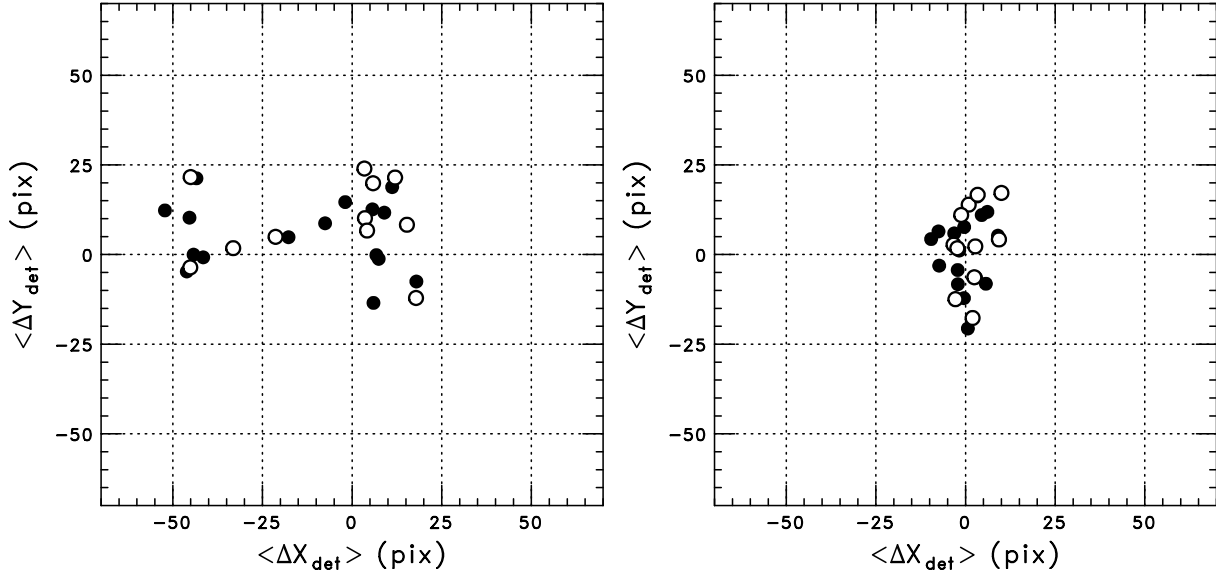
Fig. 3. (Left) Offsets of XIS source positions from the nominal positions: $\langle \Delta X_{\mathrm{det}} \rangle$ versus $\langle \Delta Y_{\mathrm{det}} \rangle$. 1 pixel $\simeq 1.04''$. Aim points of the observations are placed at the XIS nominal position (filled circles) or at the HXD nominal position (open circles). (Right) The same plot after the position correction.
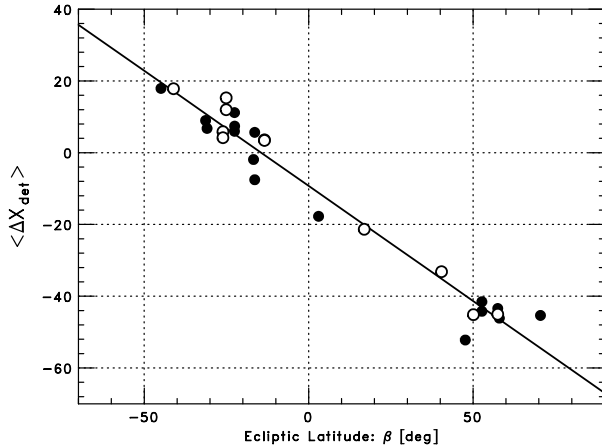
Fig. 4. Correlation between $\langle \Delta X_{\mathrm{det}} \rangle$ and the ecliptic latitude β_{ecl} of the sources.

3.2.2.   Wobbling with satellite orbital period

We next explored the wobbling motion synchronized with the orbital motion of the satellite. After inspecting correlations with various parameters stored in the satellite housekeeping data, we arrived at two parameters related with the wobbling motion. One is a difference of temperature between radiators at the side panels #8 and #6, T_86 (in units of Kelvin), defined as

$$\texttt{T\_86} \equiv \texttt{HK\_XIS\_RAD8\_T1\_CAL} - \texttt{HK\_XIS\_RAD6\_T1\_CAL}, \quad (4)$$

where HK_XIS_RAD8_T1_CAL and HK_XIS_RAD6_T1_CAL are temperatures of radiators at the side panel #8 and #6, respectively. The newly introduced parameter is found to be a good indicator of the wobbling motion in the DETX direction. The temperature difference T_86 represents a temperature gradient in side panel #7 in the DETX direction. The other parameter is the elapsed time after a night-day transition, T_DY (in units of second), defined by

$$\texttt{T\_DY} \equiv \begin{cases} \texttt{T\_DY\_NT} & \text{for day-time,} \\ -\texttt{TN\_DY\_NT} & \text{for night-time,} \end{cases} \quad (5)$$

where day-time means a period in which Sun light irradiates the satellite. We make use of the parameter T_DY to parameterize the wobbling motion in the DETY direction because it is supposed to be coupled with thermal cycling of the orbiting spacecraft.

Figure 5 shows a correlation between T_86 and ΔX_{det}, after removing the offset of $\langle \Delta X_{\mathrm{det}} \rangle$. In the plot, we utilized only bright sources with a flux higher than 2 counts s^{-1} among the samples in table 1, because the source position has to be determined for each 200-sec bin. For a fixed value of T_86 in a given observation, ΔX_{det} was found to have a scatter of about 10 pixels. We averaged ΔX_{det} for each temperature bin over each observation. There is a tendency that the source position deviates from the nominal position to the +DETX direction as the temperature difference T_86 increases. We therefore parametrized ΔX_{det} (pix) by the combination of a linear function of T_86 and $\langle \Delta X_{\mathrm{det}} \rangle (\beta_{\mathrm{ecl}})$ in equation (3) as

$$\Delta X_{\mathrm{det}} = \langle \Delta X_{\mathrm{det}} \rangle (\beta_{\mathrm{ecl}}) + 0.4 \times \texttt{T\_86}. \quad (6)$$

In figure 6 we demonstrate a correlation seen between T_DY and ΔY_{det}. It appears that ΔY_{det} increases as T_DY increase for T_DY ≤ 2000 and then starts to fall. We approximated the relation between ΔY_{det} (pix) and T_DY with a broken line:

$$\Delta Y_{\mathrm{det}} = \begin{cases} 10 + 0.007 \times \texttt{T\_DY} & \text{for } \texttt{T\_DY} \leq 0, \\ 10 + 0.0025 \times \texttt{T\_DY} & \text{for } 0 < \texttt{T\_DY} \leq 2000, \\ 45 - 0.015 \times \texttt{T\_DY} & \text{for } 2000 < \texttt{T\_DY}. \end{cases} \quad (7)$$

These empirical relations give an instantaneous deviation from the nominal position at each event time for a given observation, thus allowing corrections in the DETY direction. Note however that the absence of a direct measurement of the cross frame temperatures makes the corrections difficult.
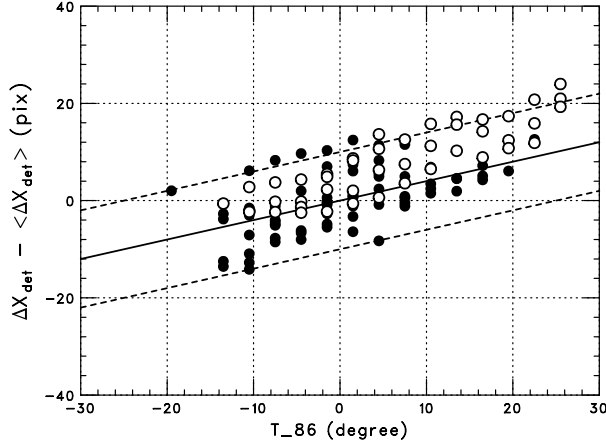
Fig. 5. Correlation between `T_86` and $\Delta X_{\mathrm{det}} - \langle \Delta X_{\mathrm{det}} \rangle$, derived by tracking the wobbling motion of bright sources. The filled points correspond to the XIS nominal cases and the open circles to the HXD nominal. The solid line represents equation (6), and the dashed lines show a range of scatter in $\langle \Delta X_{\mathrm{det}} \rangle$.
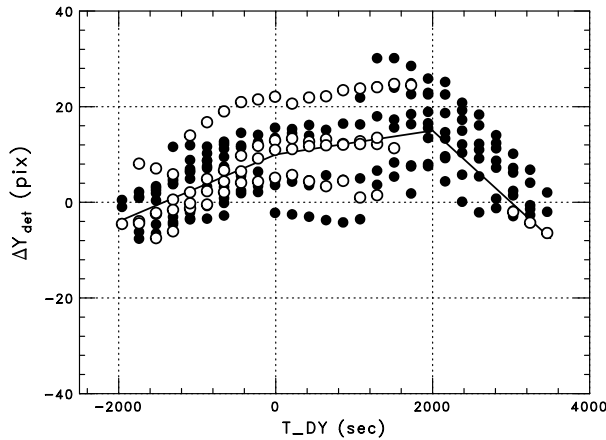
Fig. 6. Correlation between `T_DY` and ΔY_{det}. The filled points correspond to the XIS nominal cases and the open circles to the HXD nominal. The function defined by equation (7) is drawn.

4. Software Implementation

We have developed a program, `aeattcor`, to correct the parameters of the satellite attitude using the parameterization of drift of the XIS image described above.

The program first calculates the expected deviation of the XRT pointing direction from that aimed at each event

time using equations (6) and (7). The deviation corresponds to the error of the satellite attitude caused by any misalignment between the XRT-XIS system and the attitude control system. The program calculates Euler angles of the satellite attitude for the XRT-XIS system from those monitored on the attitude control system, and then updates the attitude file in which the Euler angles are stored. If one simply converts detector coordinates (DETX, DETY) to sky coordinates (X,Y) using the updated attitude file, the corrected sky coordinates (X,Y) can be obtained. A detailed description of the conversion scheme is given by Ishisaki et al. (2007).

The program is now included in FTOOLS, the official analysis software released form the Suzaku Guest Observer Facility, and will be applied to the XIS event files released through the pipeline processing V2.0 or the later versions.

5. Demonstration

In this section we demonstrate the developed program, `aeattcor`, in application to the XIS images of sample sources. We show how degree the program improves the PSF and the position accuracy.

5.1. Restored Image and PSF

The left panel of figure 7 shows time-integrated XIS-0 image of Her X-1 before the attitude-error correction, as extracted from the V1.2 event files. The image before the attitude-error correction looks as if there are two point-like sources separated by $30''$. It is because the position of Her X-1 is oscillated with the satellite orbital period, and the source visibility is limited in selected orbital phases for Earth occultation (see figure 2).

The right panel of figure 7 is an image after the attitude-error correction. One can realize that the deviation of the peak from the nominal position is improved, and the double-peak profile of the image before the correction disappears in the corrected image. In figure 2, we present a time sequence of the source position after the correction, where the large amplitude in the DETY is reduced.

To quantify the improvement of the PSF core, we introduce a new parameter, "core sharpness" S, defined as the ratio of the averaged count per pixel within an inner circle of 10-pix radius to that within an outer annulus between 10-pix and 20-pix radii. Here we determined the source centroid by fitting with a 2-dimensional Gaussian function. If the PSF is perfectly flat within 20 pixels from the center, the core sharpness is 1.0. For the instantaneous PSF free from the time-variable pointing direction, we expect $S \simeq 2$. We note that the "core sharpness" depends on each XIS because each XRT has a slightly different PSF. We here present the results of XIS-0.

Figure 8 shows the distributions of S for the sources listed in table 1, before and after the attitude-error correction. The sources with a flux higher than 50 counts exposure^{-1} chip^{-1} are shown separately with red histograms, because those bright sources are expected to severely suffer from pileup effects. It is clear that the
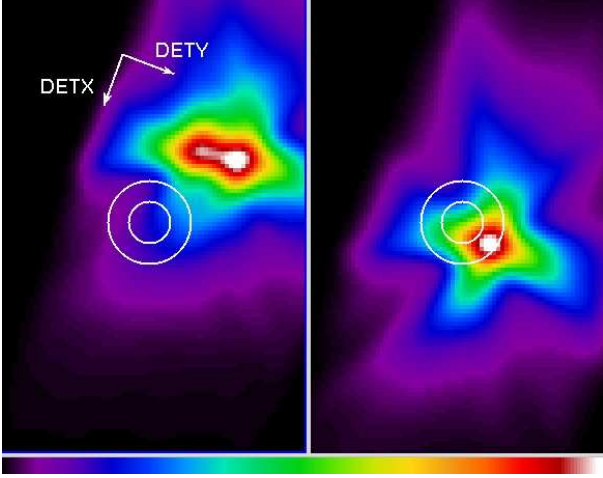
Fig. 7. Time-integrated XIS-0 images made with (X, Y) columns of Her X-1 are displayed before (left) and after (right) the position correction. Counts per pixel normalized at the peak are shown on a linear color scale. North (+Y) is up and west (+X) is to the right. The double circles with a radius of $10''$ and $20''$ show the nominal (expected) position of the source. The source peak in the corrected image in the right panel is closer to the nominal position. Furthermore, a fake double-core of the original image is clearly converged.

PSFs of the corrected image are sharpened and the core sharpness becomes close to 2, the value expected for the PSF free from the attitude error.
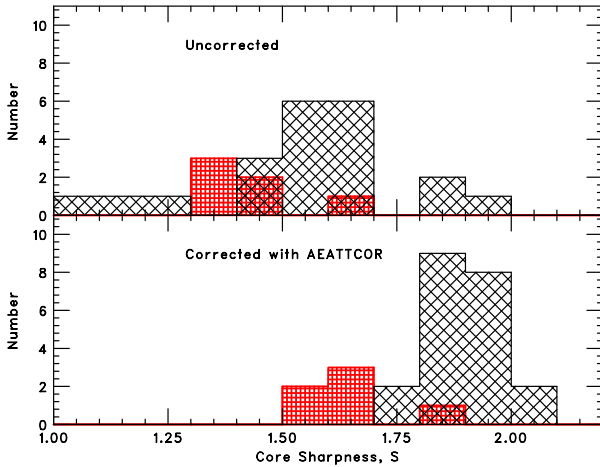

Fig. 8. Distributions of core sharpness S for XIS-0. The top panel shows the distribution of S before the correction, while the bottom panel shows that after it. $S = 1$ corresponds to a flat PSF in the central 20-pix and $S = 2$ to the undistorted PSF core. Results for bright sources exceeding 50 counts exposure^{-1}, which are likely to be affected by photon pile-up, are separately shown in red.

5.2. Improved Position Accuracy

We determined the offset of the source centroid from the expected position for all sample sources before/after the attitude-error correction, in order to evaluate the im-

provement on the source position accuracy. The distributions of these offsets ($\langle \Delta X_{\text{det}} \rangle, \langle \Delta Y_{\text{det}} \rangle$) before/after the attitude-error correction are plotted separately in figure 3. The improvement of the position accuracy is clearly seen from the difference of the two distributions.

To quantify the position accuracy, figure 9 shows the distributions of $\Delta r \equiv \sqrt{\langle \Delta X_{\text{det}} \rangle^2 + \langle \Delta Y_{\text{det}} \rangle^2}$, i.e., the distance between the source centroid and the expected position, separately before/after the attitude-error correction. Without the attitude-error correction, the deviation from the nominal position has a 90% error circle of $\Delta r \simeq 50''$ radius. The `aeattcor` restores the pointing accuracy to $\Delta r \leq 19''$ (a 90% error circle). The improvement is brought mainly by the successful parameterization of the large DETX offsets. The residual position error after the attitude-error correction is somewhat worse compared with the preflight specification, $\sim 10''$, and the position accuracy of ASCA, $\simeq 12''$ (Gotthelf et al. 2000). Given a lack of direct measurements of the temperatures of the cross frames, which are the most relevant parameters, we do not expect that further improvements can be easily made. We will monitor the Suzaku pointing accuracy to check its validity over the course of the mission.
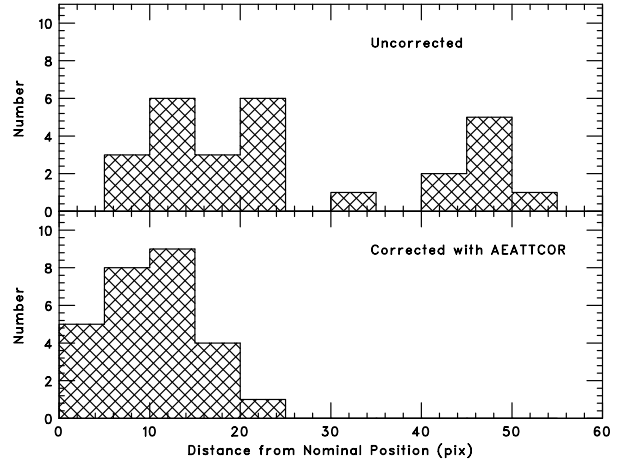
Fig. 9. Distributions of the source distance Δr from the nominal position. The top panel shows the Δr distribution before the attitude-error correction, while the bottom panel shows that after correction.

6. Summary

We have developed an empirical method to restore the position accuracy and the PSF in the observed Suzaku XIS image. We analyzed 27 pointing observations of point-like sources using the XIS-0 data of the pipeline processing V1.2 to investigate the characteristics of the drift of the XIS image which degrades the position accuracy and the PSF. We found that the deviation of the source centroid from the expected position, averaged over one pointing observation, can be well characterized by the relation between the deviation in the DETX direction and the ecliptic latitude of the pointing target. It is also found

that the oscillation of the source position synchronized with the satellite orbital period can be parameterized to some extent by the temperatures of the onboard radiators and the elapsed time since the night-day transition of the satellite. Based on the parameterization of the drifts of the XIS image, we have implemented new software, `aeattcor`, to correct the XRT pointing direction with respect to the attitude control system at each event time. By applying the attitude-error corrections to the XIS data of our sample, we demonstrated that the distorted core of PSF can be sharpened and showed that a 90% error circle of the sky position of a point-like source is reduced to $19''$ in radius. The results presented in this paper describe the current accuracy of performing astrometry with the Suzaku XIS.

References

Gotthelf, E. V., Ueda, Y., Fujimoto, R., Kii, T., & Yamaoka, K. 2000, ApJ, 543, 417

Ishisaki, Y., et al. 2007, PASJ, 59, S113

Kelley, R., et al. 2007, PASJ, 59, S77

Koyama, K., et al. 2007, PASJ, 59, S23

Mitsuda, K., et al. 2007, PASJ, 59, S1

Serlemitsos, P. J., et al. 2007, PASJ, 59, S9

Takahashi, T., et al. 2007, PASJ, 59, S35

Takei, D., et al. 2007, PASJ, this issue

Ueda, Y., Ishisaki, Y., Takahashi, T., Makishima, K., & Ohashi, T. 2001, ApJS, 133, 1

Ueda, Y., Ishisaki, Y., Takahashi, T., Makishima, K., & Ohashi, T. 2005, ApJS, 161, 185

Table 1. List of Suzaku Point Sources Used in This Study

Object	Suzaku Sequence #	R.A. (J2000.0)	Decl. (J2000.0)	$\beta_{\rm ecl}$ (deg)	Aim[*]	$\theta^\dagger$ (deg)	$\Delta X_{\rm cor}$ (pix)	$\Delta Y_{\rm cor}$ (pix)	ΔX (pix)	ΔY (pix)
MCG−6−30-15	100004010	13 35 53.80	−34 17 44.0	−22.5	XIS	296.0	13.4	−0.3	21.8	−1.8
Cen A	100005010	13 25 27.60	−43 01 08.8	−31.3	XIS	303.9	6.2	4.6	14.7	−0.9
1A 0535+26	100021010	05 38 54.57	26 18 56.8	3.0	XIS	83.6	2.3	−7.6	−6.8	−17.1
NGC 2110	100024010	05 52 11.40	−07 27 22.0	−30.9	XIS	103.4	8.5	−0.1	−1.4	6.6
NGC 3516	100031010	11 06 47.50	72 34 07.0	58.0	XIS	148.9	−0.6	9.9	41.9	−19.8
Her X-1‡	100035010	16 57 49.83	35 20 32.6	57.5	XIS	249.6	14.0	−8.7	35.1	33.3
Mkn 3	100040010	06 15 36.30	71 02 15.0	47.6	XIS	71.8	−7.1	−7.8	−28.0	−45.8
Her X-1‡	101001010	16 57 49.83	35 20 32.6	57.5	HXD	67.9	−12.6	6.1	−37.0	−33.6
PKS 2155−304	101006010	21 58 52.00	−30 13 32.0	−16.8	XIS	57.9	−6.7	0.5	−13.4	6.2
AE Aquarii	400001010	20 40 09.16	−00 52 15.1	16.9	HXD	264.9	3.0	3.1	6.8	20.8
GX 349+2‡	400003010	17 05 44.50	−36 25 23.0	−13.4	HXD	85.7	−2.1	2.9	−9.8	4.3
GX 349+2‡	400003020	17 05 44.50	−36 25 23.0	−13.4	HXD	78.9	−15.7	6.5	−22.9	8.0
SS Cyg	400006010	21 42 42.80	43 35 09.9	52.7	XIS	276.6	−4.5	1.7	−5.5	41.2
SS Cyg	400007010	21 42 42.80	43 35 09.9	52.7	XIS	256.9	1.5	1.5	10.0	43.1
X1630−472‡	400010050	16 34 01.10	−47 23 34.4	−25.1	HXD	107.7	−6.8	7.6	−12.6	12.1
X1630−472‡	400010060	16 34 01.10	−47 23 34.4	−25.1	HXD	120.3	−19.9	0.0	−24.6	−0.5
4U 1626−67	400015010	16 32 16.80	−67 27 43.0	−44.9	XIS	103.0	11.9	2.3	3.3	19.1
CH Cyg	400016020	19 24 33.07	50 14 29.1	70.5	XIS	185.8	−8.5	−6.1	46.2	−5.7
3C 120	700001020	04 33 11.10	05 21 15.0	−16.4	XIS	237.5	6.9	−9.7	7.6	−11.6
3C 120	700001030	04 33 11.10	05 21 15.0	−16.4	XIS	262.5	7.4	6.6	9.6	6.3
MCG−5−23-16	700002010	09 47 40.10	−30 56 56.0	−41.1	HXD	118.4	14.6	10.1	2.2	21.4
NGC 4051	700004010	12 03 09.60	44 31 53.0	40.4	HXD	135.3	2.7	6.2	22.3	−24.6
NGC 2992	700005020	09 45 42.00	−14 19 35.0	−26.1	HXD	88.8	−11.1	−1.0	−19.8	6.3
NGC 2992	700005030	09 45 42.00	−14 19 35.0	−26.1	HXD	128.5	0.1	−2.9	−7.8	−0.9
MCG−6−30-15	700007020	13 35 53.80	−34 17 44.0	−22.5	XIS	102.4	20.0	5.1	11.9	8.7
MCG−6−30-15	700007030	13 35 53.80	−34 17 44.0	−22.5	XIS	102.4	5.7	4.3	−0.4	7.5
0836+710	700010010	08 41 24.30	70 53 42.0	50.1	HXD	294.8	−12.5	−2.7	−22.2	39.5

Notes.—Units of right ascension are hours, minutes, and seconds, and units of declination are degrees, arcminutes, and arcseconds. $\Delta X_{\rm cor}$ and $\Delta Y_{\rm cor}$ are pixel deviations of the source centroid from the nominal position in the corrected X/Y image, while ΔX and ΔY are for the uncorrected image.
[*] Aim point of the observation. XIS: the target is placed at the nominal optical axis of the XIS. HXD: the target is placed at the nominal optical axis of the HXD, which is shifted in DETX by $-3'.5$ from the XIS optical axis.
† Roll angle in the observation, stored as PA_NOM in the header of the event FITS files.
‡ These sources have > 50 counts exposure^{-1} (0.4–10 keV) and consequently show photon pile-up in the central regions (within about 20 pixels from the center) of the PSF.